NRIAG JOURNAL OF ASTRONOMY AND GEOPHYSICS
2021, VOL. 10, NO. 1, 372–386
https://doi.org/10.1080/20909977.2021.1938884

Study of trend and fluctuations of global solar radiation over Egypt

M.L. Eladawy[a], H. A. Basset[a], Mostafa Morsy[a] and M. H. Korany[b]

[a]Department of Astronomy and Meteorology, Faculty of Science, Al-Azhar University, Cairo, Egypt; [b]Egyptian Meteorological Authority, Kobry Al-Qubbah, Cairo, Egypt

ABSTRACT

Climatological spatiotemporal variability of global solar radiation (GSR) and its trend analysis, fluctuations and abrupt changes based on seven sites (Cairo, Arish, Barrani, Matrouh, Aswan, Asyut, Kharga) in Egypt were studied during the period 1985–2018. Fifth-generation dataset of European Center for Medium-Range Weather Forecasts (ECMWF) reanalysis of the global climate and weather for the past 4 to 7 decades (ERA5) data after validation with available observed GSR data has been used. Monthly, seasonal and annual GSR values have marked variations. The results revealed that the highest values of coefficient of variation occurred at stations in winter, while the lowest values occurred in summer. Moreover, in winter and spring, all stations presented a positive Mann-Kendell (MK) trend and almost all stations in annual except Aswan, Asyut and Kharga, whereas in autumn, all station presented a negative MK trend, summer in all stations except Barrani and Cairo. The fluctuations in the annual GSR were investigated using the cumulative sum charts (CUSUM) method, where all stations have alternating trend between negative and positive CUSUM along period.

ARTICLE HISTORY
Received 2 March 2021
Revised 4 May 2021
Accepted 1 June 2021

KEYWORDS
Global solar radiation (GSR); GSR spatiotemporal variation; trend analysis; cumulative sum charts (CUSUM); abrupt change; Egypt

1. Introduction

The spatiotemporal characterisation of available solar radiation variability is important for the successful grid integration of photovoltaic (PV), especially in developing countries like Egypt. The global solar radiation (GSR) drives the global energy, water and carbon cycles by affecting latent and sensible heat fluxes, water vapour, longwave emission and circulations in the ocean and the atmosphere (Wang et al. 2010; Wild et al. 2013, 2017). Assessing the variations and trend of GSR is necessary for understanding the global climate changes, especially the rate of global warming and its effects on glacial melt and sea level rise (Wild et al. 2007; Yang et al. 2011). GSR data are urgently required in many application fields, such as agricultural meteorology, global numerical weather prediction, PV panels and climate monitoring. Moreover, the accuracy of GSR data mostly influences evapotranspiration computation, simulations of runoff and growth and yield of crops (Jia et al. 2013; Mokhtari et al. 2018; Rap et al. 2018; M. Zhang et al. 2011). GSR represents the sum of the direct (DNI) and the diffuse (DHI) components of solar radiation that fall together on a horizontal surface; these basic solar components or GSR are of interest to concentrating PV systems. Currently, GSR products are available from four sources, namely, ground measurements of surface radiation networks (Wild et al. 2017), simulations based on radiation transfer models (Mondol et al. 2008), estimates from reanalysis systems (Xia et al. 2006; Hersbach 2017) and retrievals from satellite observations (Greuell et al. 2013; Nikitidou et al. 2015; Huang et al. 2019). Ground measurements are regarded as a reliable reference for data validation from simulations, reanalysis and satellite retrievals (Jiang et al. 2020; Y. Wang et al. 2018). However, these radiation products generally contain large uncertainties. The reported root-mean-square error (RMSE) of instantaneous Rs retrievals under all-sky conditions range from 60 to 140 W/m^2 (~15–30%) depending on local cloud climatology (Huang et al. 2019). In addition, multisource products usually show inconsistent temporal trends and spatial distributions (Huang et al. 2019; X. Zhang et al. 2015), which could hamper their applicability for assessing global brightening or dimming and local climate responses to radiation changes. In Egypt, Basset et al. 2007 studied the relationships between the GSR and UV-B radiation at four stations in Egypt, thereby deducing empirical formulas for estimating UV-B from global radiation at these stations (Basset and Korany 2007).

The analysis of solar radiation over Egypt conducted by Omran showed the effects of high levels of

CONTACT M.L. Eladawy mohamed_eladawy@azhar.edu.eg

air pollution in Cairo, the coastal climate at Matrouh and the low latitude climate at Aswan on the solar climate of each of the stations relative to the other two stations. These differences were summarised in the following points:

- Global radiation at Cairo was in the order of that in the region, while the direct radiation, either normal incidence or on horizontal surface, was relatively lower, but diffuse radiation was relatively higher than that in the other two stations.
- The statistical analysis showed that large values of hourly global irradiation (2 MJ m^2) had a maximum of eight hours per day in both June and July, all over the country, but this never occured at Matrouh and Cairo in January and December (Omran 2000).

Robaa provided methods for estimating global and diffuse solar radiation, as well as direct solar radiation with high accuracy at any location in Egypt. This is useful for the design of various systems utilising solar energy (Robaa 2003). The significant spatiotemporal difference of data accuracy mainly results from atmospheric parameters, such as total cloud cover, total column water vapour and aerosol optical depth. Since solar radiation measurement stations are challenging to operate and the data collected are not used for routine weather forecasts, they are few and have limited data collection records. Although the measured data are the best form of this knowledge, there are very few meteorological stations that measure GSR, especially in developing countries like Egypt. Despite the presence of some previous studies that studied some aspects of different solar radiation components over Egypt, the study of the solar radiation variation in time and space in Egypt has not received enough research studies. The aim of this work is to study the trend and fluctuations of GSR over Egypt. This goal will be accomplished by validating the ERA5 dataset with the measured GSR data of the seven stations and testing the homogeneity of this data. The fluctuations in the behaviour of GSR data at the seven stations, the coefficient of variation (COV), cumulative sum charts (CUSUM) and abrupt changes have been applied and analysed during the period 1985–2018 over Egypt.

2. Study area and stations

Egypt covers an area of about 1,000,000 km^2, located between latitudes 22 and 32°N and longitude between 25 and 37°E (Figure 1). The geographical location of Egypt in the southeastern part of

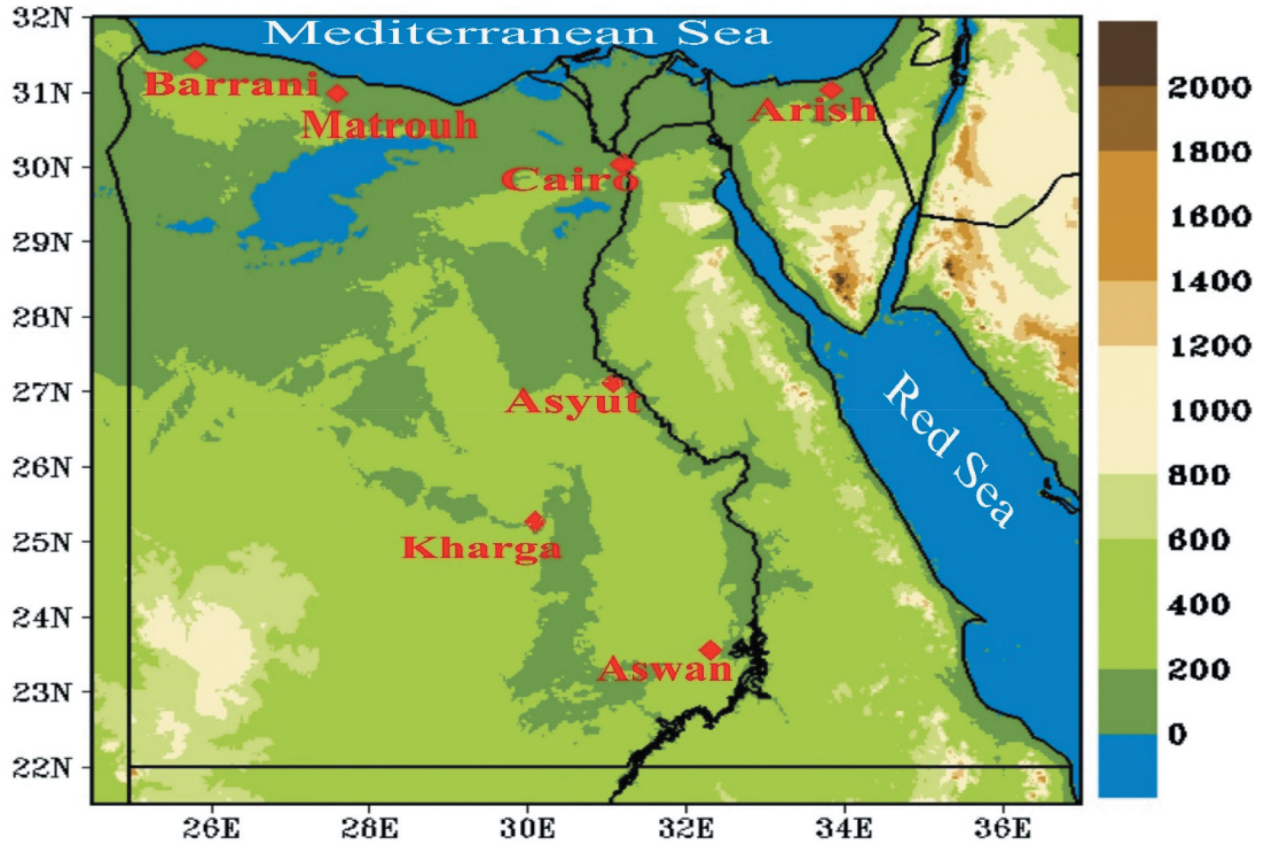

Figure 1. The locations of the selected seven stations and the topography of Egypt.

Table 1. Geographical information for the selected seven stations and data availability and average elevation (metres above sea level).

Station	WMO No.	Latitude (°N)	Longitude (°E)	Elevation (m)	Available period
Barrani	62,301	31.38	25.24	24	1985–2007
Matrouh	62,306	31.20	27.13	25	1985–2017
Arish	62,337	31.18	33.30	30	1985–2015
Cairo	62,371	30.05	31.17	35	1985–2002
Asyut	62,392	27.12	31.30	52	1985–2010
Kharga	62,435	25.27	30.35	78	1985–2010
Aswan	62,414	23.58	32.47	192	1985–2007

the Mediterranean basin and the occupation of the desert by more than 90% of its lands make it globally and locally vulnerable to different climatic characteristics as seasons change. Where the Mediterranean climate prevails in the northern part, and the desert and semi-desert climate prevails in the southern part (Aboelkhair et al. 2019), and its summers are hot and dry, while its winters are mild with irregular rainfall (Domroes and El-Tantawi 2005). Solar energy is the main source that drives and controls the Earth's climate system, where seasons occur as a result of changes in the intensity and duration of solar energy due to the various sun positions and the tilt of the Earth's axis (Lam and Li 1999). Seven meteorological radiation stations (Barrani, Matrouh, Arish, Cairo, Asyut, Aswan and Kharga) were selected to cover all different climatic regions in Egypt. Figure 1 illustrates the locations of these stations and the topography (coloured) of Egypt, while Table 1 contains the geographical information (WMO station number, latitude, longitude and elevation) for these stations and the data availability. Three of these stations (Arish, Barrani and Matrouh) are coastal stations, generally influenced by the Mediterranean climate, and located at about 1–10 km south of the Mediterranean Sea coast and the soil is generally sandy. Cairo (semi-arid warmer dry climate with a broad summer dry season) is located in the Nile Delta and the land is generally clay. Aswan is about 2 km away from Nasser Lake to the east and the land is generally sandy but with granite rocks, while Asyut lies near the Nile River to the west and the soil is sandy, and Kharga is in the western desert and the soil is clay rocks. Besides, Asyut, Aswan and Kharga are characterised by dry desert climate and lie in low latitude region. It is also noticed that Aswan station has the highest altitude (192 m) followed by Kharga (78 m), while has the lowest altitude (17 m) and the rest five stations have the range of altitudes from 24 m (Barrani) to 52 m (Asyut) as shown in Table 1. Furthermore, Cairo, Asyut and Aswan stations are located along the Nile river; Barrani and Matrouh are in the northwestern part of Egypt; Kharga is in the middle of southern Egypt; and Arish is in northeastern part of Egypt (north of Sinai Peninsula).

3. Data and methodology

3.1. Data used

The observed data used are grouped into two sets of data. The first set of data is a collection of observed data from the synoptic stations of Egypt that belongs to the Egyptian Meteorological Authority (EMA). Monthly and annual mean GSR data for seven stations located in the study area are used over the historical period of 34 years (1985–2018). These climate stations are presented in Figure 1 with detailed geographic information provided in Table 1. However, some stations had incomplete data and shorter duration than the 34 years recommended. Due to the lack of GSR data measured in the stations of our study area, the second set of reanalysis data is provided by ERA5 database on regular latitude–longitude grids at 0.25 * 0.25 resolution from 1979 to present, available at https://climate.copernicus.eu/climate-reanalysis (Hersbach 2017). The fifth-generation (EAR5) dataset which is provided by the European Center for Medium-Range Weather Forecasts (ECMWF) atmospheric reanalysis of the global climate is used in this study. ERA5 is produced using a 4D-Var assimilation system of ECMWF's Integrated Forecast System (IFS), namely IFS Cycle 41r2, which guarantees significant increase in forecast accuracy and computational efficiency. The advanced system is also combined with vast amounts of historical observations to generate globally consistent time series of multiple climate variables. ERA5 provides hourly estimates of many atmospheric, land-surface and sea-state parameters together with their uncertainties at reduced spatial and temporal resolutions. The monthly mean parameter used in this study is "surface solar radiation downwards", which represent the amount of shortwave radiation (surface direct and diffuse solar radiation), reaching the surface of the Earth. Estimates of surface solar radiation downwards can be derived by adding total sky direct solar radiation to diffuse solar radiation.

3.2. Comparison between ERA5 and observed data

Figure 2 shows an example of the observed data (solid blue line) and ERA5 data (dotted red line) for the monthly GSR at Arish station, which shows their convenience and compatibility. Arish station was chosen for this comparison (Figure 2) because it has longer observation records (1985–2017) than other selected stations. As illustrated in Table 2, ERA5 dataset provides a reliable and accurate GSR data at all

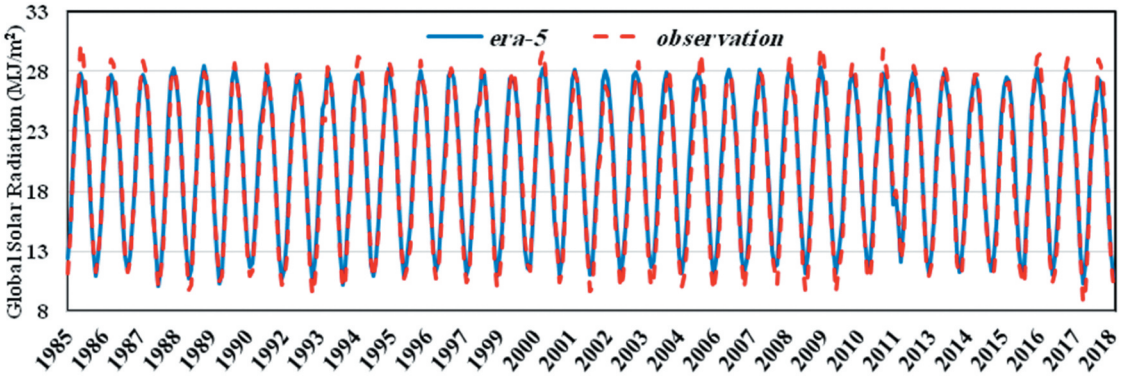

Figure 2. Comparison between ERA5 (dotted red line) data and its corresponding observed (solid blue line) data for the monthly global solar radiation parameter at Arish station.

Table 2. R^2, RMSE, MBE and MPE% for the global radiation between ERA5 and observed data at the selected seven stations in Egypt.

Station	R^2	RMSE	MBE	MPE
Barrani	0.959	1.63	0.93	0.25
Matrouh	0.9749	1.34	0.92	0.23
Arish	0.9774	1.07	0.57	0.17
Cairo	0.9689	2.21	1.39	0.34
Asyut	0.9577	1.98	1.27	0.30
Kharga	0.96	1.78	1.22	0.27
Aswan	0.9693	1.38	1.07	0.24

stations, where the minimum coefficient of determination (R^2) is 0.9577 at Asyut, while the maximum RMSE of 2.21 MJ/m^2, Mean Bias Error (MBE) of 1.39 MJ/m^2 and Mean Percentage Error (MPE) of 0.34% are recorded in Cairo station. Thus, the accuracy of ERA5 data for GSR is accepted and has a high compatibility with observations at all stations.

3.3. Methodology

The methodology applied in this study includes computation of monthly, seasonal and annual averages from the daily GSR data. In addition, the homogeneity test, COV, trend analysis, fluctuations, abrupt change and the cumulative annual means were applied in the GSR historical data. These statistical analysis procedures were performed in order to identify the spatial and temporal variations of solar radiation over Egypt under climate change conditions. The applied statistical methods in this study are described as follows:

3.3.1. Homogeneity of the data

The homogeneity of the GSR data is assessed using Bartlett's homogeneity test, where the Gaussian distribution is considered. This homogeneity test is mainly performed by dividing the climate time series into K equal sub-periods, where k must be equal to or greater than 2. This method is designed to examine the equality of variance of data between these different sub-periods, where the sample variance S_k^2 is calculated as in Eq. 1 (Mitchell et al. 1966).

$$S_k^2 = \frac{1}{n}\left(\sum x_i^2 - \frac{1}{n}\left(\sum x_i\right)^2\right), \quad (1)$$

where S_k^2 is the sample variance, x_i^2 is the score for observation in each sub-period, n is the number of observations in each sub-period and k is the number of sub-periods. The climate period of 33 years (1986–2018) is chosen from the available GSR data to perform the homogeneity test and divided into three sub-periods (K = 3), each sub-period has 11 years (n = 11, sample size). Also, the critical value of S_{max}^2/S_{min}^2 at 95% significance point can be obtained from the values given in Biometrika table 31 (Pearson and Hartely 1958), where S_{max}^2 and S_{min}^2 represent the maximum and the minimum values of sample variance S_k^2, respectively.

3.3.2. The coefficient of variation (COV)

The COV for the GSR data at each station has been estimated from Eq. (2).

$$COV = \frac{SD}{m} * 100, \quad (2)$$

where SD represents the standard deviation and m is the mean of the data along the period of study.

3.3.3. Trend analysis and fluctuations

To assess the statistical significant trends and analyse the spatial and temporal variations and fluctuations in the annual and seasonal data for GSR at each station, as well as over Egypt during the period 1985–2018, the non-parametric Mann-Kendall (MK) test is applied (Sneyers 1990; Schönwiese and Rapp 1997; Hasanean 2004; Smadi and Zghoul 2006). This trend analysis method is scientifically significant and is widely used to detect trends in various data, such as climate, hydrological and water resource data (Mavromatis and Stathis 2011; Jaiswal et al. 2015), and it is recommended by the World Meteorological Organization (WMO) in time-varying analysis of environmental data (Mitchell et al. 1966; Yue et al. 2002). Also, it does not require a normal data distribution and has low sensitivity to abrupt breaks due to inhomogeneity

in the time series (Tabari et al. 2011). The sequential steps to estimate the MK rank statistics used in this research are described in detail by Smadi and Zghoul (2006). Furthermore, the Gaussian (Mitchell et al. 1966) and Binomial (Mitchell et al. 1966; Tyson et al. 1975) low-pass filters (smooth) are used to reveal the underlying trends and features in the annual GSR data.

3.3.4. Cumulative sum charts (CUSUM)

To study the fluctuations or persistence in the behaviour of annual GSR data at the study's seven stations, CUSUM procedure is applied (Taylor 2000a, 2000b; Smadi and Zghoul 2006). The advantage of this method is the detection of time-varying structures in the GSR time series and performing a change point analysis, where the sudden changes in the direction of CUSUM indicate a sudden shift in the average. The CUSUM charts are produced by calculating the cumulative amount and plotting it based on the time series of the GSR data as follows:

The average of the GSR values ($\bar{x}$) can be calculated using Eq. 3.

$$\bar{x} = \frac{1}{n}\sum_{i=1}^{n} x_{i,} \tag{3}$$

where x_i is the annual GSR values, n is the number of years (n = 1, 2, 3, 4, ..., N) and N is the total number of available years.

Then, the cumulative sum starts at zero and calculates other cumulative sums by adding the difference between current value (x_i) and the average ($\bar{x}$) to the previous sum repeatedly as in Eq. 4.

$$\text{CUSUM}_{\ i} = \text{CUSUM}_{\ i-1} + (x_i - \bar{x}) \tag{4}$$

3.3.5. Abrupt change (Tests for Change Point Detection)

The detection of the change points (abrupt changes) is very important to determine when a significant change has occurred in the time series data. Pettit's test (Pettitt 1979) is applied for abrupt changes detection in the GSR time series. This non-parametric test was used in several studies as a useful technique for examining the occurrence of abrupt changes in climatic records (Cleugh et al. 2007; Gao et al. 2011; Smadi and Zghoul 2006; Sneyers 1990; Tarhule and Woo 1998; Verstraeten et al. 2006; Zhang and Lu 2009). It is also a common test for change point detection due to its sensitivity to breaks in the middle of any climate or time series datasets (Wijngaard et al. 2003). The test was described by Pettitt (1979) and explained by several studies (Smadi and Zghoul 2006; Suhaila et al. 2008; Štěpánek et al. 2009; Kang and Yusof 2012; Ahmad and Deni 2013). Moreover, a change point analysis can be considered as a powerful tool to determine whether a change has occurred and its frequency, and when that change has occurred.

4. Results

4.1. Homogeneity of the data

Non-climatic (e.g. station relocations, changes in instrumentation, urbanisation, observation times and methods, exposure and estimating and measuring technique) or man-made changes affect climate observations and cause homogeneities in the historical record of climate data (Costa and Soares 2009; Badawy et al. 2017; Kamel et al. 2017). Therefore, assessing the quality of observations and the homogeneity of long climate records is a very important procedure before they are reliably used to study long-term trends and natural variability of climate data. Several homogenisation techniques have been developed to detect and adjust non-climatic in homogeneities. In this study, Bartlett's test for homogeneity of variances (described in Section 3) is used to assess the homogeneity of annual and seasonal GSR data at the selected seven Egyptian stations. By considering K = 3 and n = 11, the critical value of the ratio S^2_{max}/S^2_{min} at 95% significance point is 4.85. The Bartlett homogeneity test result for the annual and seasonal GSR at all study stations is shown in Table 3. By comparing the obtained critical value of the ratio S^2_{max}/S^2_{min} (4.85) with the results in Table 3, one can notice that the mean annual GSR data appear to be homogeneous at all stations.

4.2. Monthly and seasonal horizontal distribution of GSR

Figure 3 shows the horizontal distribution of the monthly mean GSR during the period from 1985 to 2018 over Egypt. Generally, Figure 3 illustrates that GSR increases gradually from north to south of Egypt for all the months of the year with a clear difference in the values of GSR between North and South Egypt for each month, so the gradient in the values of GSR differ from month to month. In winter, it is found that the highest value of GSR for December in the south is 17.5 MJ/m^2, while the lowest value in the north is 10.5 MJ/m^2, and then the range is 7 MJ/m^2,

Table 3. Bartlett test for the annual and seasonal global solar radiation at the selected seven reanalysis ERA5 stations with ratio (S^2_{max}/S^2_{min}) 4.85 at 95% significant point for K = 3 and n = 11.

Station	Annual	Winter	Spring	Summer	Autumn
Barrani	0.10	0.02	0.43	0.25	0.38
Matrouh	0.31	0.03	1.8	0.37	0.13
Arish	0.02	0.01	0.77	0.19	0.07
Cairo	0.12	0.01	0.89	0.42	0.06
Asyut	0.02	0.11	0.21	0.16	0.09
Kharga	0.07	0.22	0.41	0.19	0.10
Aswan	0.16	0.05	0.45	0.19	0.07

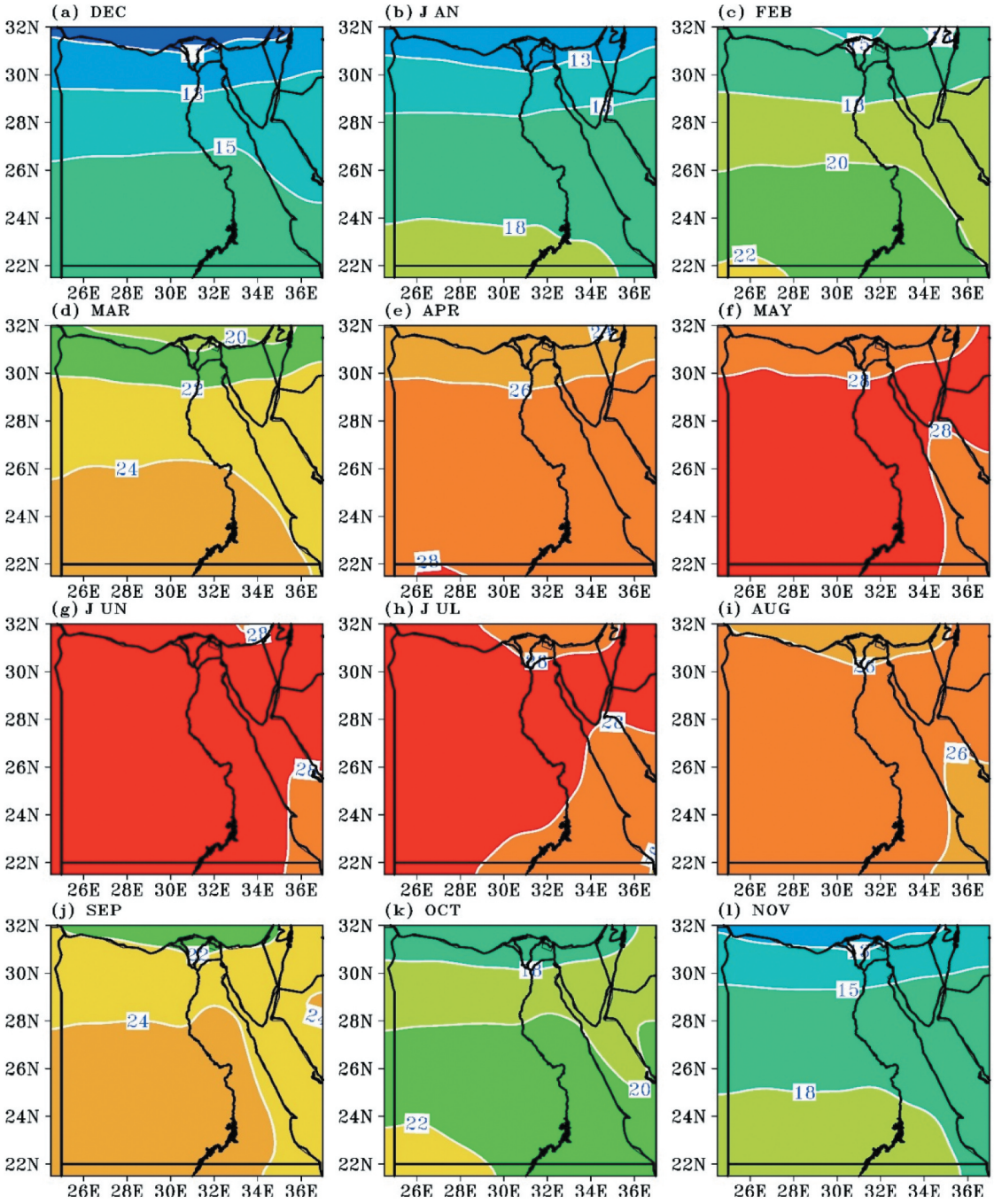

Figure 3. Horizontal distribution of monthly global solar radiation data over Egypt.

while in January, the lowest value of GSR in the north is 12 MJ/m^2, and the highest value in the south is 18.5 MJ/m^2 and the range is 6.5 MJ/m^2. In February, the lowest value in the north is 15 MJ/m^2 and the highest value in the south is 22 MJ/m^2 and the range is 7 MJ/m^2. In spring, the values of GSR begin to increase gradually from March (25–20 MJ/m^2) until they reach their highest values in May (27–28.5 MJ/m^2). The range between the highest and lowest values in summer months is very small. The pattern of the horizontal distribution of GSR in summer is different from that in winter and autumn, where the higher values occur over the southwest part of Egypt. The lines of equal GSR are zonal in winter and autumn, while the pattern of the horizontal distribution of GSR in autumn months is similar to that of winter, with higher values in September and lower values in November. The maximum range between the higher values of GSR in south and the lower values in north appears in November (13 MJ/m^2). Figure 4 shows the horizontal distribution of the seasonal mean GSR during the period from 1985 to 2018 over Egypt. It illustrates that the lower values of GSR occurs in winter and it ranges between 13.5 MJ/m^2 at the north and 19.5 MJ/m^2 at the south of Egypt. The second lower seasonal GSR values appear in autumn and it ranges between 17 and 22 MJ/m^{2}from north to south of Egypt, respectively. The higher

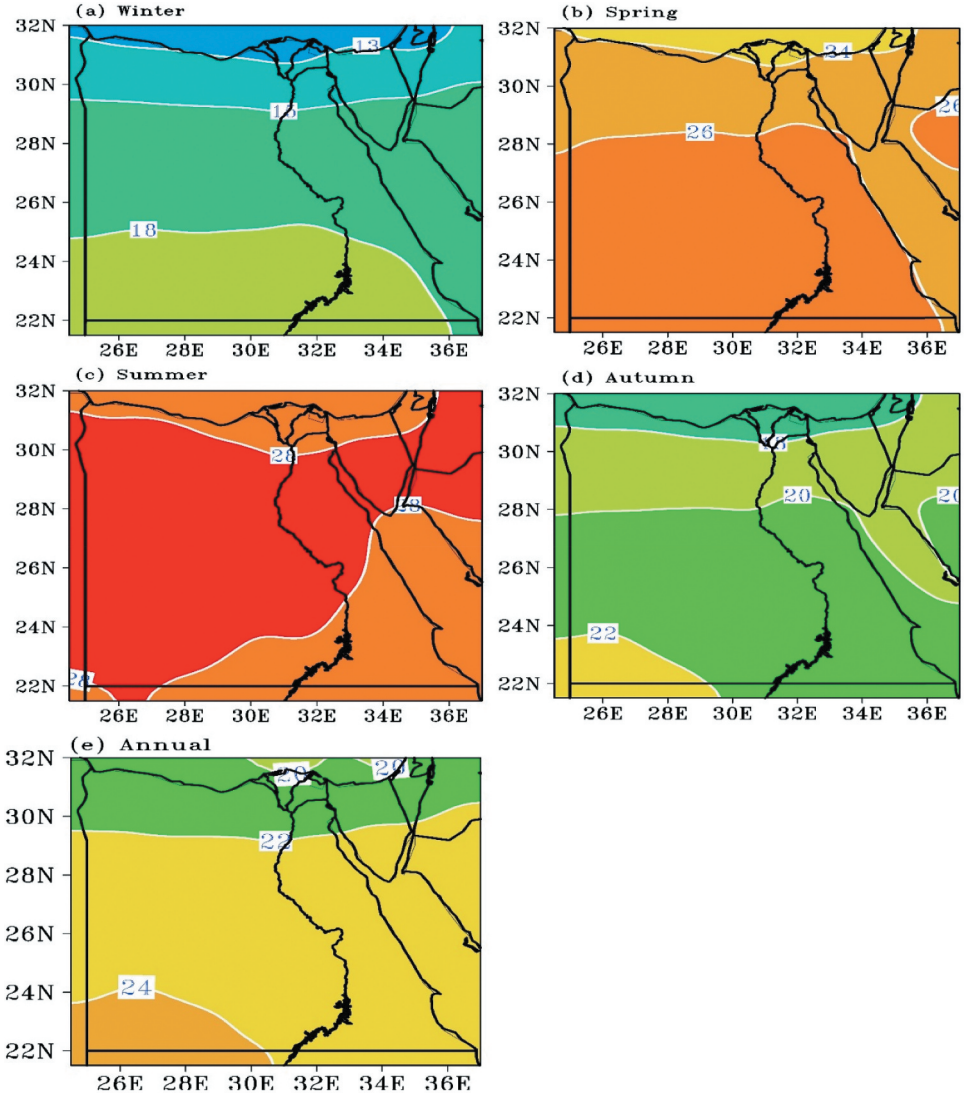

Figure 4. Horizontal spatial distribution of seasonal and annual global solar radiation over Egypt.

values of GSR occur in summer and it ranges between 27 MJ/m^2 at the north and 28.5 MJ/m^2 at the south of Egypt.

In each pattern (Figures 3 and 4), one can notice that the Nile Delta region mostly has the lowest GSR values. This is mainly due to the high concentration level of air pollution and aerosols (Saber et al. 2020) produced from the existing industrial areas (e.g. Helwan and Shobra El-Keima), about 4 million vehicles, and a population of about 30 million people. At the rest of Egypt area, the GSR values may decrease during periods of cloudy and sand or dust storm conditions. Moreover, the GSR often reaches the maximum in southwestern Egypt due to the low latitudes, while Arish has a relatively high GSR value, which indicates that it mostly has a clear atmosphere (Omran 2000). GSR varies from one month or season to another due to the atmospheric transparency changes. During winter (December, January and February), middle latitude weather conditions are prevalent, and the cloud types are normally opaque to the direct solar radiation beam and the turbidity of the atmosphere is low (Omran 2000). The spring (March, April and May) is characterised by small-scale frequent-chained depressions (Khamsin phenomena) moving across the Great Sahara generally associated with hot, dry and dusty weather (Omran 2000; El-Wakil et al. 2001), which relatively reduces the GSR values. During autumn (September, October and November), the atmosphere is moderately transparent, and the perceptible water vapour has the maximum values, where the fog, mists and low clouds form at morning and rapidly dissipate after sunrise (Omran 2000) that clearly reduce the GSR values. In summer (June, July and August), the subtropical high and Indian monsoon low are the dominant pressure systems (Saber et al. 2020), and the sky is often dirty due to the presence of fine dust particles associated with the continental tropical air (Omran 2000). Furthermore, the summer relative humidity is small (50–15%) compared to other seasons (Saber et al. 2020) and the dust content decreases significantly when Mediterranean air arrives (El-Metwally 2005), which makes GSR in summer greater than the other

seasons. Lastly, Omran (2000) summarised the solar radiation over Egypt in the following points: First, GSR at Cairo is in the order of that in the region, while the direct radiation, on horizontal surface, is relatively low, but diffuse radiation is relatively higher than other stations. Second, the statistical analysis shows that large values of hourly global radiation (2 MJ m^2) has a maximum of eight hours per day in both June and July, all over the country, but this never occurs at Matrouh and Cairo in January and December. Third, daily global radiation is high in Aswan all over the year, while it is high in Matrouh and Cairo during the period of July to October.

Table 4. The COV for the seasonal and annual GSR at the seven ERA5 stations.

Station	Annual	Winter	Spring	Summer	Autumn
Barrani	1	4	2	1	2
Matrouh	1	4	2	1	2
Arish	1	2	2	1	1
Cairo	1	3	2	0.5	2
Asyut	1	2	1	0.5	1
Kharga	0.5	1	1	0.5	1
Aswan	0.5	1	1	1	1

4.3. Coefficient of variation (COV)

The variability in solar radiation that reaches any point on the Earth's surface depends and significantly is influenced by weather conditions (such as atmospheric compositions, aerosols and clouds), the geographical location and change in the position of the sun from sunrise to sunset as well as the change in the distance of the Sun–Earth during different seasons and throughout the year (Lam and Li 1999; Domroes and El-Tantawi 2005; Wainaina and Sato 2018). The annual and seasonal COV for GSR at the selected seven ground-based stations is shown in Table 4.

The highest COV in GSR at all stations occurs during winter (as a result of active weather conditions), followed by spring and autumn, while the lowest COV is found mostly during annual and summer. Barrani, Matrouh and Cairo stations have the maximum COV in GSR either during seasons or annual.

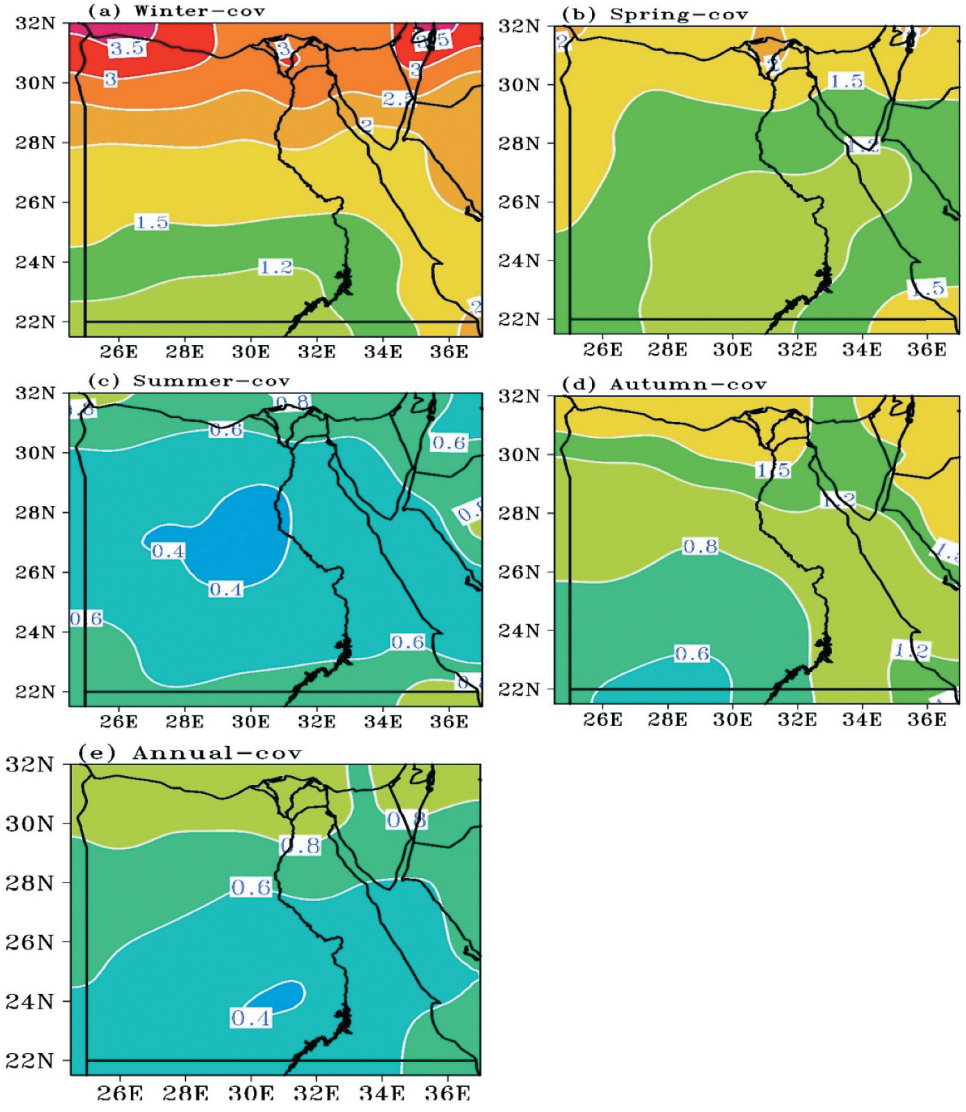

Figure 5. Horizontal distribution of COV for the seasonal and annual GSR.

The maximum COV during winter is noticed at Matrouh and Barrani. These results are clearly shown by the horizontal distribution of COV for annual and seasonal GSR (Figure 5). Figure 5 illustrates that the values of COV in both annual and seasons decrease gradually from north to south of Egypt, where the lowest COV values in both annual and seasons are detected over the desert and arid areas (south and southwest Egypt), which are mostly due to the clear sky throughout the year. On the other hand, the largest COV values are noticed in the Nile Delta, Gulf of Suez and Mediterranean and Red Sea coasts, which are generally due to the active weather condition (northward oscillation of the surface Red Sea trough and the travelling Mediterranean cyclones), aerosols and heavy air pollution, resulting from human activities in these regions. Moreover, Nile Delta region and middle Egypt in autumn have largest COV values (about 3) because of the harvest, biomass burning and increased fuel combustion in late autumn (Saber et al. 2020). The COV gradient during both annual and seasons range from about 0.4 to about 4, where the highest gradient is perceived in the middle and northern Egypt. S. M. ROBAA (2006) found that the monthly mean of GSR shows that the standard deviation has relatively high values in May (±3.27) and April (±3.13) compared with the small values of June (±0.96) and July (±0.91). This may be attributed to the strong fluctuation in the density of atmospheric dust particles, resulting from Khamsin depressions during spring season (March to May).

4.4. Gaussian and binomial low-pass filters for the annual GSR

A significant and widespread decrease in surface solar radiation (global dimming) occurred from the 1950s to the 1980s, after which a recovery (global brightness) occurred (Wild et al. 2005; Wild 2012). To study the annual GSR brightness and dimming, the trend analysis of the GSR annual mean at the considered seven ground-based stations is applied using the Gaussian and binomial low-pass filters as shown in Figure 6. It is noticed that there is a yearly variation in the GSR trend at different sites during the period 1985–2018. It is also detected that there is a decreasing trend (dimming) in the GSR at the beginning of the period, especially in the 1990s at all stations. During this dimming period, the GSR decreased below the trend average (dashed line) by about 0.4–0.6 MJ/m^2 at the different stations. Additionally, minor increases in GSR trend are detected in the mid-1990s at most stations. Moreover, from both the Gaussian (dotted line) and binomial (solid line) trends in Figure 6, one can notice that the GSR increased (brightness) from the middle of the 2000s to about 2015, except kharga and Asyut to about 2012 and decreased again during the end of the period at most stations. Generally, the GSR reaches to its peak during 2009 at the northern stations Barrani (20.57 MJ/m^2), Matrouh (20.64 MJ/m^2), Arish (20.26 MJ/m^2) and Cairo (21.37 MJ/m^2) and 2000 at Asyut (22.91 MJ/m^2), Kharga (23.62 MJ/m^2) and 1986 at Aswan (23.68 MJ/m^2). In contrast, the lowest GSR values occurred in 1992 at all stations: Cairo (20.81 MJ/m^2), Aswan (23.38 MJ/m^2), Kharga (23.35 MJ/m^2), Asyut (22.53 MJ/m^2), Barrani (20.07 MJ/m^2), Matrouh (20.16 MJ/m^2) and Arish (19.88 MJ/m^2). On the other hand, the maximum GSR trend value is 23.68 MJ/m^2 at Aswan among the southern stations and 20.64 MJ/m^2 at Matrouh among the northern stations, while its minimum value is 22.53 MJ/m^2 at Asyut among the southern stations and 19.88 MJ/m^2 at Arish among the northern stations. Furthermore, from Figure 6, it is found that the annual mean (dashed line) of the GSR trend at the southern stations (Asyut, Kharga and Aswan) is greater than the northern stations (Arish, Matrouh, Barrani and Cairo), where the annual mean for Aswan, Kharga and Asyut (southern stations) are 23.58, 23.53 and 22.78 MJ/m^2, respectively, while for Arish, Matrouh, Barrani and Cairo are 20.11, 20.42, 20.34, 21.13 MJ/m^2, respectively.

Finally, the behaviour of the annual time series (1985–2018) of the GSR trend can be divided into three distinct periods at all stations: two periods of 1985–1998 and 2015–2018 in which a decreasing GSR trend occurs and one period 2000–2015 in which an increased GSR trend occurs.

4.5. Mann-Kendall (MK) rank statistical test

The MK rank statistical test results for the annual and seasonal GSR at the seven ground-based stations are shown in Table 5. It is interesting to note that most stations present positive trends (increasing in GSR) for both annual and seasonal GSR, while the negative trends (decreasing in GSR) occurred over Arish (summer and autumn), Aswan, asyut and Kharga (annual, summer and autumn). Moreover, in winter and spring, all stations presented a positive MK trend and almost all stations in annual, except Aswan, asyut and Kharga, whereas in autumn, all stations presented a negative MK trend, summer in all station, except Barrani and Cairo. The spatial distribution pattern of MK test for the seasonal and annual GSR over Egypt along the period 1985–2018 is given in Figure 7. Table 5 and Figure 7 show that the negative MK trend values are dominated for the annual in the southeastern of Egypt (Asyut, Aswan, Kharga stations), as well as in summer and winter. Regarding the MK positive trends, all Egypt area has a positive trend in winter and spring followed by summer, except Matrouh, Arish,

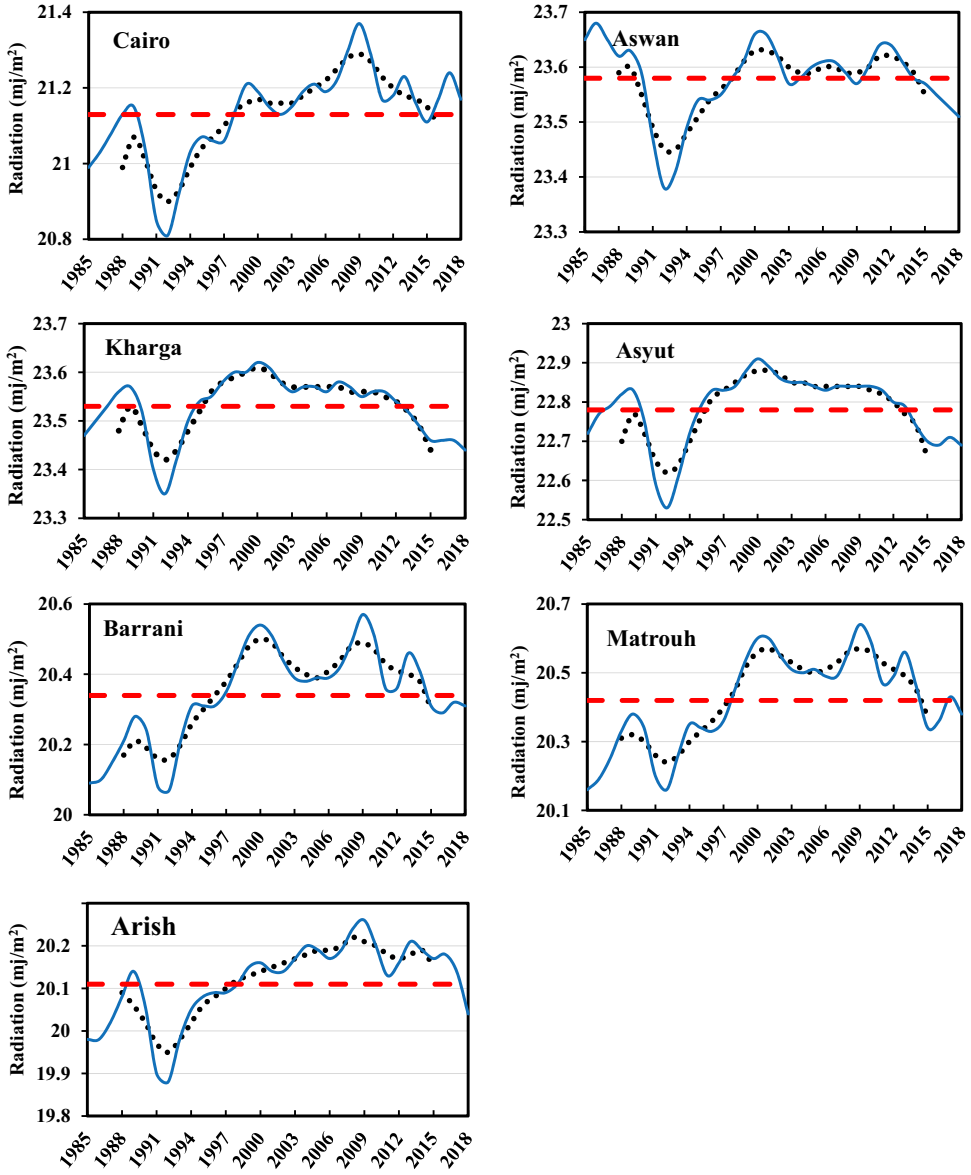

Figure 6. Gaussian (dotted line) and binomial (solid line) low path filter-trend and their average (dashed line) for the GSR over the considered seven stations.

Table 5. Mann-Kendall trend for the annual and seasonal GSR at ERA5 stations.

Station	Annual	Winter	Spring	Summer	Autumn
Barrani	.24064	.10160	.22638	.00178	−.00178
Matrouh	.27273	.19430	.22638	−.10517	−.00178
Arish	.27629	.27629	.18717	−.10873	−.01604
Cairo	.20499	.24064	.14082	.03743	−.02317
Asyut	−.00535	.13012	.00891	−.18360	−.20499
Kharga	−.06952	.11943	.06595	−.22995	−.14082
Aswan	−.03387	.01248	.08021	−.27986	−.01961

Aswan, asyut and Kharga. In annual, the positive trend area is detected in the middle, north and northwest, except south of Egypt, while in autumn, it is noted that all of Egypt are a negative trend. It is clear from Table 5 and Figure 7 that the maximum annual and seasonal MK trend occurred at Cairo station followed by Barrani, while the minimum MK trend occurred at Kharga, Aswan and Cairo in annual, summer and autumn (the lowest), respectively. Generally, the MK trend in both annual and seasons decreases gradually southward in all stations, except summer and autumn.

4.6. Cumulative sum charts (CUSUM)

The CUSUM method is used to clarify the fluctuations or persistence and the long-term variability in the behaviour of the annual GSR at the seven ground-based stations across the period 1985–2018. The CUSUM have smoothing effects, such as low pass filters, and help to identify the alternating increases or decreases in the annual time series of the GSR. Figure 8 illustrates the CUSUM (solid line) and its climate averaged (dashed line) for the annual GSR time series at all stations, where a period where

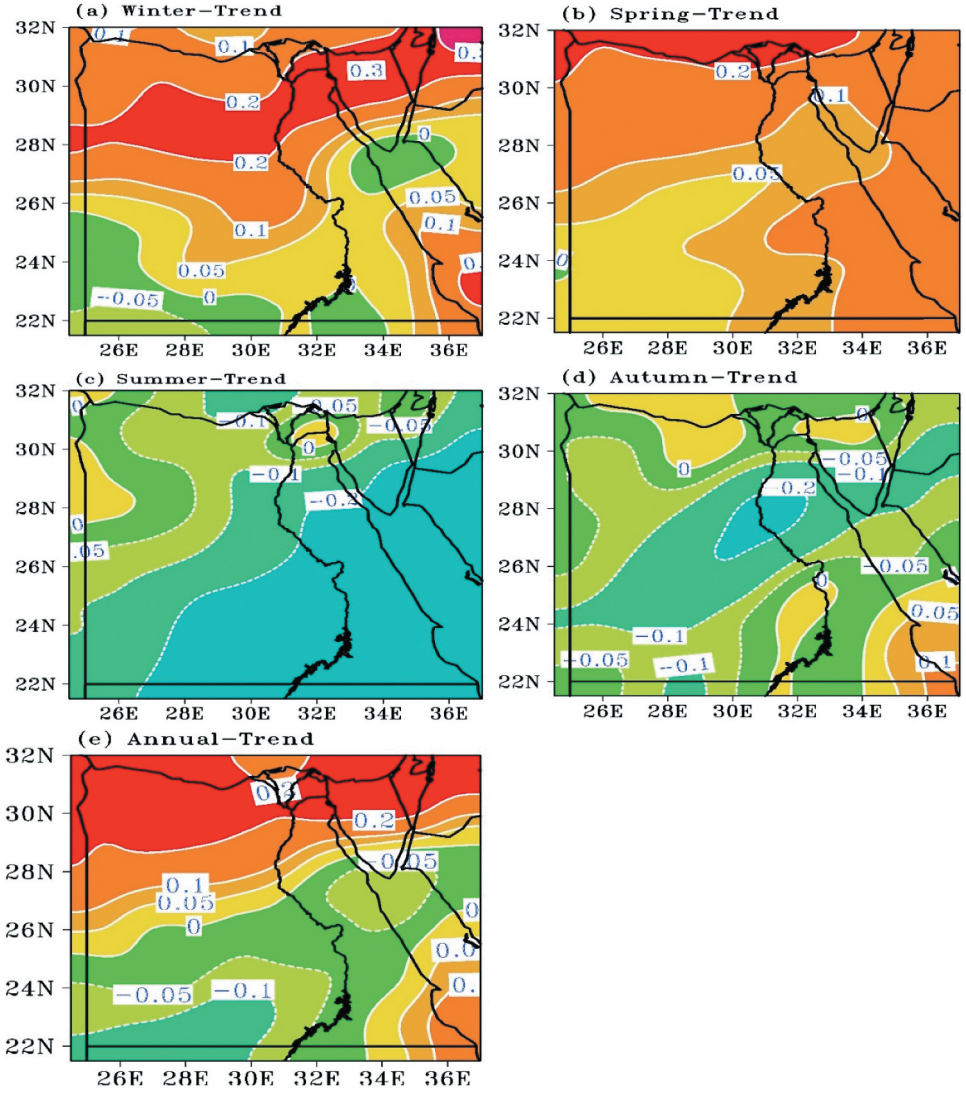

Figure 7. Spatial distribution of MK trend for the annual and seasonal GSR over Egypt.

the CUSUM chart follows a relatively straight path indicates a period where the average does not change. It is found that all stations have alternating trend between negative and positive CUSUM along the study period. For Barrani and Matrouh stations, negative CUSUM occurred during the period 1985–2000 and the positive CUSUM is detected during the period 2000–2018. The CUSUM for Arish and Cairo have the same behaviour throughout the study period, where they have a negative value during the period 1985–1989 followed by positive values during the period 1989–1991 and decreased again from 1991–2003 followed by increase up to 2018. Also, the CUSUM for Asyut and Kharga station is negative during the period 1985–1988 followed by positive until 1988–1991 and returned to the negative during the period 1991–2000 followed again by positive up to 2018. In addition, the maximum climate average of the CUSUM (dashed line) is noticed in Aswan (23.58 MJ/m^2) followed by Kharga (23.52 MJ/m^2) and Asyut (22.76 MJ/m^2), while the minimum CUSUM climate average is detected in Arish (20.06 MJ/m^2) followed by Barrani (20.25 MJ/m^2), Matrouh (20.33 MJ/m^2) and Cairo (21.07 MJ/m^2). Finally, one can notice that the CUSUM climate average for the annual GSR in the southern stations (Asyut, Kharga and Aswan) is greater than that in the northern stations (Cairo, Barrani, Matrouh and Arish).

4.7. Abrupt change analysis

The detection of sudden irregular changes (abrupt changes) and climate jumps in the GSR data during the period 1985–2018 at all stations of the study is identified using the change point detection procedure as shown in Figure 9. It is obvious that the GSR values appear to be outsideof the control limits due to the frequent abrupt changes that occurred during the study period. The first change point occurred with an increase in the GSR values (positive abrupt change) at all stations, where this

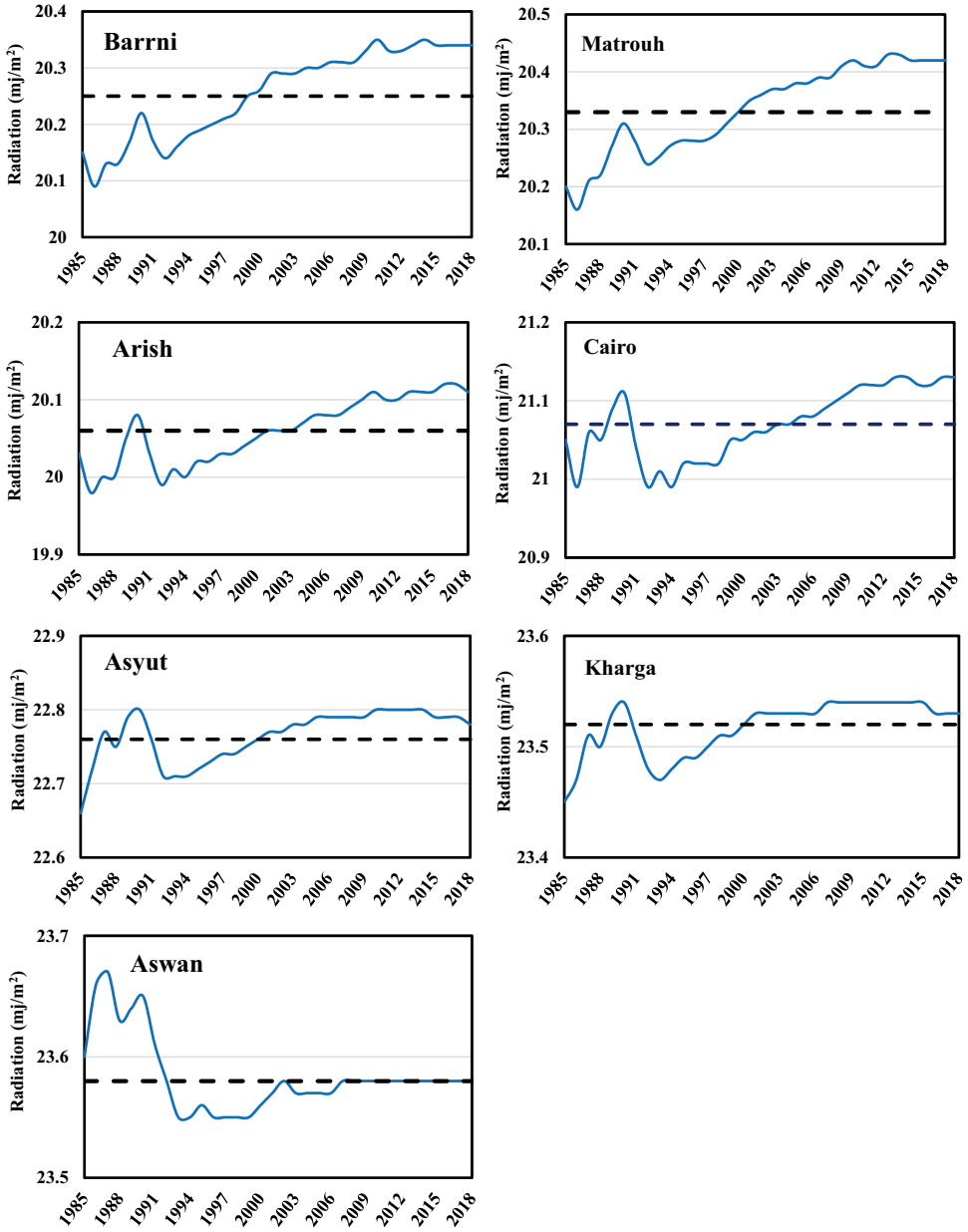

Figure 8. The cumulative sum charts (solid line) and its climate average (dashed line) for the annual GSR at all stations.

first change point is present in the 1999, except Barrani Kharga and Aswan in 1997, 1998 and 2000, respectively. The second (only at Barrani, Arish and Cairo) change points are positive with an increase in the GSR values in 2007, 2008 and 2008, respectively, whereas the negative abrupt change points with decreases in GSR occurred at all stations, except Cairo (Arish and Matrouh) during 2018 and 1992, 2014, 2015 and 2016 for Aswan, Kharga, Asyut and Barrani, respectively. The second change point occurred in 2018 only at Aswan station.

5. Conclusion

GSR is considered to be one of the most important meteorological parameters, which plays an important and vital role in various sectors and applications (solar energy systems, buildings, agriculture, etc.). The spatiotemporal and statistical variations of the monthly, seasonal and annual GSR at seven stations (Barrani, Matrouh, Arish, Cairo, Asyut, Aswan and Kharga) in Egypt during the climate period 1985–2018 were analysed, investigated and discussed. The observed GSR data were obtained from the EMA and have different recording periods and some missing values at each station. Thus, the EAR5 dataset for the GSR from ECMWF was used to fill this lack and missing data, where it provides an accurate GSR data with high coefficient of determination (>0.95) and small bias and percentage errors at all stations. In addition, the Bartlett's homogeneity test revealed that the annual and seasonal completed GSR data are homogeneous at all selected stations. It is concluded that the GSR is varying from

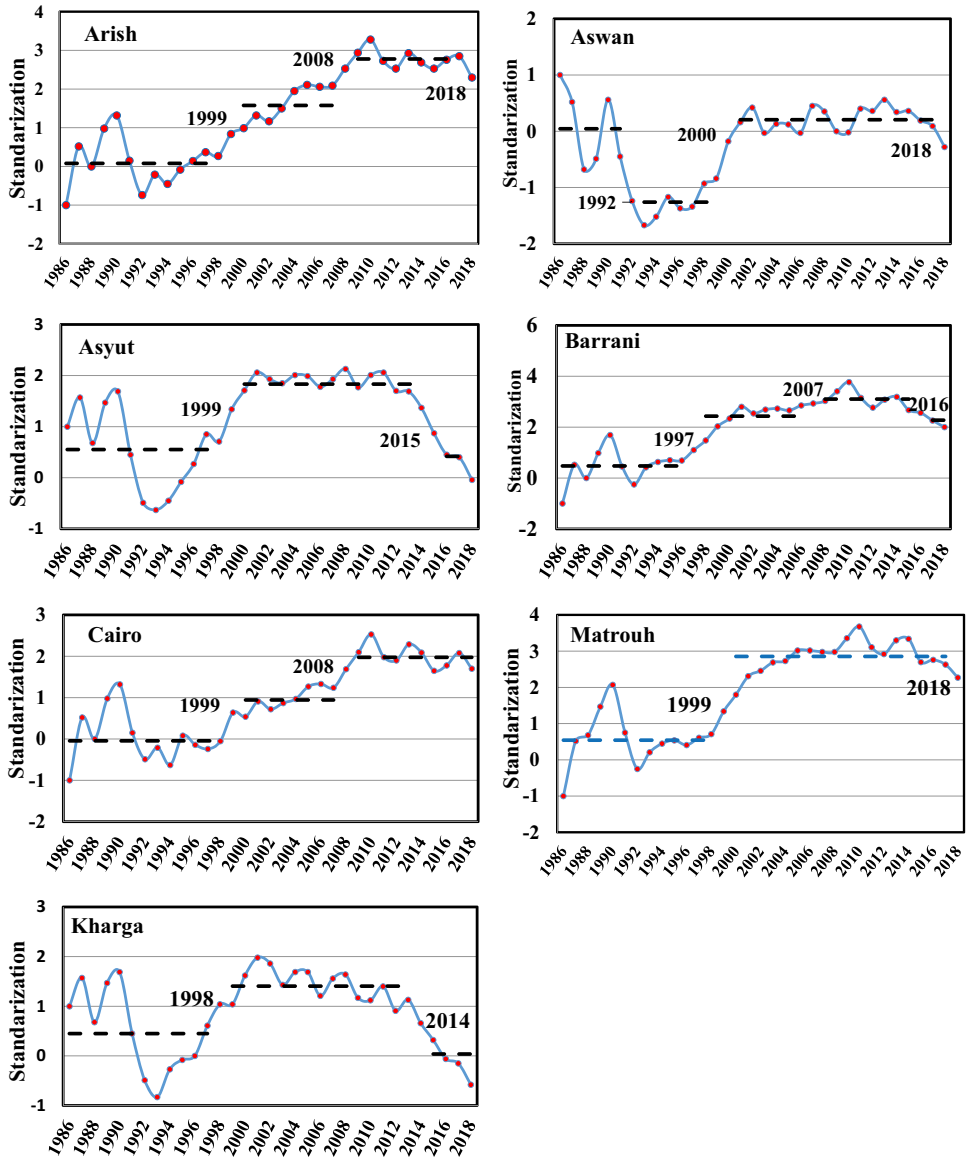

Figure 9. Shifts in the mean for abrupt change standardisation of the annual GSR data at all stations (Probability = 0.1, cut-off length = 10, Huber parameter = 1).

lowest in December (10.5 MJ/m^2) and winter (12.5 MJ/m^2) to June (29.5 MJ/m^2) and summer (28.5 MJ/m^2). Generally, the monthly, seasonal and annual GSR have a marked variation and gradually increase southward (function of latitude) and often reach to the maximum values in the southwest of Egypt. Furthermore, it is found that the highest COV for the GSR occurred in winter at all stations followed by spring, autumn and summer, respectively, as well as the COV values decrease gradually southward. It is also concluded that most stations present a positive trend (increasing in GSR), except some negatives (decreasing in GSR) at different stations during different seasons, where all Egypt area has a positive trend in winter and spring followed by summer, except Matrouh, Arish, Aswan, asyut and Kharga. On the other hand, the first abrupt change point occurred (positive abrupt change) at all stations in 1999, except Barrani Kharga and Aswan in 1997, 1998 and 2000, respectively. The second positive abrupt change point occurred only at Barrani, Arish and Cairo and detected in 2007, 2008 and 2008, respectively. Moreover, the negative abrupt change points occurred at Arish, Matrouh Aswan, Kharga, Asyut and Barrani in 2018, 1992, 2014, 2015 and 2016, respectively, while the second change point occurred only at Aswan in 2018. Finally, this research has contributed to the body of knowledge in terms of determining the most exposed places to solar radiation in Egypt. Hence, recommendations for new places to construct solar-based power generation plants are provided.

Disclosure of potential conflicts of interest

No potential conflict of interest was reported by the authors.

ORCID

Mostafa Morsy http://orcid.org/0000-0002-0271-2074

References

Aboelkhair H, Morsy M, El Afandi G. 2019. Assessment of agroclimatology NASA POWER reanalysis datasets for temperature types and relative humidity at 2 m against ground observations over Egypt. Adv Space Res. 64 (1):129–142. doi:10.1016/j.asr.2019.03.032.

Ahmad NH, Deni SM. 2013. Homogeneity test on daily rainfall series for Malaysia. Matematika. 29(1):141–150. http://www.matematika.utm.my/index.php/matematika/article/view/586

Badawy A, Abdel Basset HA, Eid M. 2017. Spatial and temporal variations of total column ozone over Egypt. Journal of Earth and Atmospheric Sciences. 2(June):1–15.

Basset HA, Korany MH. 2007. The global and UV-B radiation over Egypt.Atmósfera 20(4):341–358.

Cleugh HA, Leuning R, Mu Q, Running SW. 2007. Regional evaporation estimates from flux tower and MODIS satellite data. Remote Sens Environ. 106(3):285–304. doi:10.1016/j.rse.2006.07.007.

Costa AC, Soares A. 2009. Homogenization of climate data: review and new perspectives using geostatistics. Math Geosci. 41(3):291–305. doi:10.1007/s11004-008-9203-3.

Domroes M, El-Tantawi A. 2005. Recent temporal and spatial temperature changes in Egypt. Int J Climat. 25 (1):51–63. doi:10.1002/joc.1114.

El-Metwally M. 2005. Sunshine and global solar radiation estimation at different sites in Egypt. J Atmos Sol-Terr Phys. 67(14):1331–1342. doi:10.1016/j.jastp.2005.04.004.

El-Wakil SA, El-Metwally M, Gueymard C. 2001. Atmospheric turbidity of urban and desert areas of the Nile Basin in the aftermath of Mt. Pinatubo's eruption. Theor Appl Climatol. 68(1–2):89–108. doi:10.1007/s007040170056.

Gao P, Mu XM, Wang F, Li R. 2011. Changes in streamflow and sediment discharge and the response to human activities in the middle reaches of the Yellow River. Hydrol Earth Syst Sci. 15(1):1–10. doi:10.5194/hess-15-1-2011.

Greuell W, Meirink JF, Wang P. 2013. Retrieval and validation of global, direct, and diffuse irradiance derived from SEVIRI satellite observations. J Geophys Res Atmos. 118 (5):2340–2361. doi:10.1002/jgrd.50194.

Hasanean HM. 2004. Variability of the North Atlantic subtropical high and associations with tropical sea-surface temperature. Int J Climat. 24(8):945–957. doi:10.1002/joc.1042.

Hersbach H 2017. News from C3S: ERA5. Using ECMWF's Forecasts, 1–27. https://www.ecmwf.int/sites/default/files/elibrary/2017/17312-news-c3s-era5.pdf .

Huang G, Li Z, Li X, Liang S, Yang K, Wang D, Zhang Y. 2019. Estimating surface solar irradiance from satellites: past, present, and future perspectives. Remote Sens Environ. 233(August):111371. doi:10.1016/j.rse.2019.111371.

Jaiswal RK, Lohani AK, Tiwari HL. 2015. Statistical analysis for change detection and trend assessment in climatological parameters. Environ Process. 2(4):729–749. doi:10.1007/s40710-015-0105-3.

Jia B, Xie Z, Dai A, Shi C, Chen F. 2013. Evaluation of satellite and reanalysis products of downward surface solar radiation over East Asia: spatial and seasonal variations. J Geophys Res: Atmo. 118(9):3431–3446. doi:10.1002/jgrd.50353.

Jiang H, Yang Y, Wang H, Bai Y, Bai Y. 2020. Surface diffuse solar radiation determined by reanalysis and satellite over East Asia: evaluation and comparison. Remote Sens. 12 (9):1–19. doi:10.3390/RS12091387.

Kamel AM, Abdel Basset H, Sayad T 2017. Rainfall analysis and variability over Egypt. Al-Azhar Bulletin of Science, 9th (Conference), 41–62.Cairo.Egypt

Kang HM, Yusof F. 2012. Homogeneity tests on daily rainfall series in Peninsular Malaysia. Int J Contemp Math Sciences. 7(1):9–22. https://www.researchgate.net/publication/267676130

Lam JC, Li DHW. 1999. An analysis of daylighting and solar heat for cooling-dominated office buildings. Solar Energy. 65(4):251–262. doi:10.1016/S0038-092X(98)00136-4.

Mavromatis T, Stathis D. 2011. Response of the water balance in Greece to temperature and precipitation trends. Theor Appl Climatol. 104(1–2):13–24. doi:10.1007/s00704-010-0320-9.

Mitchell J, Dzezerdzeeskii B, Flohn H, Hofmeyer W, Lamb H, Rao K, Wallen C 1966. Climatic change. World Meteorological Organization,Geneva, 79 (WmoTechnica 1 Note No), 79.

Mokhtari A, Noory H, Vazifedoust M. 2018. Improving crop yield estimation by assimilating LAI and inputting satellite-based surface incoming solar radiation into SWAP model. Agric For Meteorol. 250–251 (December 2017):159–170. doi:10.1016/j.agrformet.2017.12.250.

Mondol JD, Yohanis YG, Norton B. 2008. Solar radiation modelling for the simulation of photovoltaic systems. Renewable Energy. 33(5):1109–1120. doi:10.1016/j.renene.2007.06.005.

Nikitidou E, Kazantzidis A, Tzoumanikas P, Salamalikis V, Bais AF. 2015. Retrieval of surface solar irradiance, based on satellite-derived cloud information, in Greece. Energy. 90:776–783. doi:10.1016/j.energy.2015.07.103

Omran MA. 2000. Analysis of solar radiation over Egypt. Theor Appl Climatol. 67(3–4):225–240. doi:10.1007/s007040070011.

Pearson S, Hartely H. 1958. Biometrika tables for statistication. Vol. 1. New York:Cam Bridge Univ. Press; p.238.

Pettitt AN. 1979. A non-parametric approach to the change-point problem published by Wiley for the royal statistical society a non-parametric approach to the change-point problem. J R Stat Soc Ser C Appl Stat. 28 (2):126–135.

Rap A, Scott CE, Reddington CL, Mercado L, Ellis RJ, Garraway S, Evans MJ, Beerling DJ, MacKenzie AR, Hewitt CN, et al. 2018. Enhanced global primary production by biogenic aerosol via diffuse radiation fertilization. Nat Geosci. 11(9):640–644. doi:10.1038/s41561-018-0208-3.

Robaa SM. 2003. On the estimation of global and diffuse solar radiation over Egypt. MAUSAM.2(April):511–520.

ROBAA SM. 2006. A study of solar radiation climate at cairo urban area, Egypt and its environs. Int J Climat. 26 (13):1913–1928. doi:10.1002/joc.

Saber A, Abdel Basset H, Morsy M, El-Hussainy FM, Eid MM. 2020. Characteristics of the simulated pollutants and atmospheric conditions over Egypt. NRIAG J Astron Geophys. 9(1):402–419. doi:10.1080/20909977.2020.1755479.

Schönwiese C, Rapp J. 1997. Climate trend atlas of Europe based on observations. Dordrecht: Kluwer Academic Publishers; p. 228.

Smadi MM, Zghoul A. 2006. A sudden change in rainfall characteristics in Amman, Jordan during the mid 1950s. Am J Environ Sci. 2(3):84–91. doi:10.3844/ajessp.2006.84.91.

Sneyers R 1990. On the statistical analysis of series of observations. Technical Note 143, 415(Geneva), 192.

Štěpánek P, Zahradníček P, Skalák P. 2009. Data quality control and homogenization of air temperature and precipitation series in the area of the Czech Republic in the period 1961–2007. Adv Sci Res. 3(1):23–26. doi:10.5194/asr-3-23-2009.

Suhaila J, Deni SM, Jemain AA. 2008. Detecting inhomogeneity of rainfall series in Peninsular Malaysia. Asia-Pac J Atmos Sci. 44(4):369–380.

Tabari H, Somee BS, Zadeh MR. 2011. Testing for long-term trends in climatic variables in Iran. Atmos Res. 100 (1):132–140. doi:10.1016/j.atmosres.2011.01.005.

Tarhule A, Woo MK. 1998. Changes in rainfall characteristics in northern Nigeria. Int J Climat. 18(11):1261–1271. doi:10.1002/(sici)1097-0088(199809)18:11<1261::aid-joc302>3.0.co;2-z.

Taylor W. 2000a. A pattern test for distinguishing between autoregressive and mean-shift data. J Q Technol. 1–14. http://www.variation.com/files/articles/pattern.pdf .

Taylor WA 2000b. Change-point analysis: a powerful new tool for detecting changes. Taylor Enterprises, 1–19. http://www.variation.com/cpa/tech/changepoint.html .

Tyson PD, Dyer TGJ, Mametse MN. 1975. Secular changes in South African rainfall: 1880 to 1972. Q J R Meteorolog Soc. 101(430):817–833. doi:10.1002/qj.49710143008.

Verstraeten G, Poesen J, Demarée G, Salles C. 2006. Long-term (105 years) variability in rain erosivity as derived from 10-min rainfall depth data for Ukkel (Brussels, Belgium): implications for assessing soil erosion rates. J Geophys Res Atmos. 111(22):1–11. doi:10.1029/2006JD007169.

Wainaina B, Sato T. 2018. Interannual and spatial variability of solar radiation energy potential in Kenya using Meteosat satellite. Renewable Energy. 116:88–96. doi:10.1016/j.renene.2017.09.069

Wang K, Dickinson RE, Wild M, Liang S. 2010. Evidence for decadal variation in global terrestrial evapotranspiration between 1982 and 2002: 1. Model development. J Geophys Res Atmos. 115(20). doi:10.1029/2009JD013671.

Wang Y, Trentmann J, Yuan W, Wild M. 2018. Validation of CM SAF CLARA-A2 and SARAH-E surface solar radiation datasets over China. Remote Sens. 10 (12):1–18. doi:10.3390/rs10121977.

Wijngaard JB, Klein Tank AMG, Können GP. 2003. Homogeneity of 20th century European daily temperature and precipitation series. Int J Climat. 23 (6):679–692. doi:10.1002/joc.906.

Wild M. 2012. Enlightening global dimming and brightening. Bull Am Meteorol Soc. 93(1):27–37. doi:10.1175/BAMS-D-11-00074.1.

Wild M, Folini D, Schär C, Loeb N, Dutton EG, König-Langlo G. 2013. The global energy balance from a surface perspective. Clim Dyn. 40(11–12):3107–3134. doi:10.1007/s00382-012-1569-8.

Wild M, Gilgen H, Roesch A, Ohmura A, Long CN, Dutton EC, Forgan B, Kallis A, Russak V, Tsvetkov A. 2005. From dimming to brightening: decadal changes in solar radiation at earth's surface. Science. 308 (5723):847–850. doi:10.1126/science.1103215.

Wild M, Ohmura A, Makowski K. 2007. Impact of global dimming and brightening on global warming. Geophys Res Lett. 34(4):4. doi:10.1029/2006GL028031.

Wild M, Ohmura A, Schär C, Müller G, Folini D, Schwarz M, Hakuba MZ, Sanchez-Lorenzo A 2017. The Global Energy Balance Archive (GEBA) version 2017: a database for worldwide measured surface energy fluxes. Earth System Science Data Discussions, May, 1–24. 10.5194/essd-2017-28

Xia XA, Wang PC, Chen HB, Liang F. 2006. Analyis of downwelling surface solar radiation in China from national centers for environmental prediction reanalysis, satellite estimates, and surface observations. J Geophys Res Atmos. 111(9):1–9. doi:10.1029/2005JD006405.

Yang W, Guo X, Yao T, Yang K, Zhao L, Li S, Zhu M. 2011. Summertime surface energy budget and ablation modeling in the ablation zone of a maritime Tibetan glacier. J Geophys Res Atmos. 116(14):1–11. doi:10.1029/2010JD015183.

Yue S, Pilon P, Cavadias G. 2002. Power of the Mann ±Kendall and Spearman's rho tests for detecting monotonic trends in hydrological series. J Hydrol. 259(1–4):254–271. doi:10.1016/S0022-1694(01)00594-7.

Zhang M, Yu GR, Zhuang J, Gentry R, Fu YL, Sun XM, Zhang LM, Wen XF, Wang QF, Han SJ, et al. 2011. Effects of cloudiness change on net ecosystem exchange, light use efficiency, and water use efficiency in typical ecosystems of China. Agric For Meteorol. 151(7):803–816. doi:10.1016/j.agrformet.2011.01.011.

Zhang S, Lu XX. 2009. Hydrological responses to precipitation variation and diverse human activities in a mountainous tributary of the lower Xijiang, China. Catena. 77(2):130–142. doi:10.1016/j.catena.2008.09.001.

Zhang X, Liang S, Wild M, Jiang B. 2015. Analysis of surface incident shortwave radiation from four satellite products. Remote Sens Environ. 165:186–202. doi:10.1016/j.rse.2015.05.015